Tortosa, M.; Manjon, F. J.; Mollar, M.; et ál. (2012). ZnO-based spinels grown by electrodeposition. Journal of Physics and Chemistry of Solids. 73(9):1111-1115. doi:10.1016/j.jpcs.2012.04.002.

ZnO-based spinels grown by electrodeposition

M. Tortosa,* F. J. Manjón, M. Mollar, and B. Marí

Instituto de Diseño para la Fabricación y Producción Automatizada, Universitat Politècnica de València, E-46022 Valencia, Spain.

We report the synthesis of thin films of $ZnCo_2O_4$ and $ZnMn_2O_4$ spinels, as well as pure Co_3O_4 and Mn_3O_4 spinels, by means of electrodeposition. Spinel thin films have been analyzed by energy dispersive spectroscopy, X-ray diffraction, and Raman spectroscopy. We show that under certain deposition conditions, where the Co and Mn concentration in the films is above the solubility limit of these ions in the wurtzite structure, the initial wurtzite structure of Co- and Mn-doped ZnO develops into other compounds with spinel structure.

1. Introduction

Spinel oxides have a general formula $A^{II}B^{III}{}_2O_4$ in which A is a small divalent metal with tetrahedral coordination and B is a large trivalent metal with octahedral coordination. It is known that spinels containing transition metal ions can act as efficient catalysts in a number of heterogeneous chemical processes, such as CO oxidation **[1]**, catalytic combustion of hydrocarbons **[2]** or selective oxidation and reduction of several organic molecules **[3-5]**. They can also be used in Li-ion batteries **[6,7]** and in gas sensors attending the growing demand for monitoring toxic and harmful gases **[8]**.

Spinels are known to crystallize in either cubic (Fd-3m) or tetragonal ($I4_1/amd$) structures. The tetragonal spinel structure results from a distortion of the cubic spinel structure due to the deformation of octahedra as a result of Jahn-Teller interactions. In particular, Co_3O_4 ($Co^{2+}Co^{3+}{}_2O_4$) is a pure cubic spinel **[9]** while Mn_3O_4 ($Mn^{2+}Mn^{3+}{}_2O_4$) is a tetragonal spinel due to the presence of Jahn-Teller Mn^{3+} ions in octahedral sites **[10]**. Spinels are complex structures because they have unoccupied cation sites in the unit cell that lead to intrinsic disorder, called inversion, in which cations at tetrahedral and octahedral sites interchange their respective positions. Few vibrational studies of the spinel structure are reported in the literature because AO_4 and BO_6 polyhedra are very interrelated and it is difficult to interpret vibrational spectra in terms of single contributions from tetrahedral or octahedral units.

The most general method for preparing oxide spinels is the ceramic process that requires the solid-state reaction of a mixed powder of the parent metal binary oxides at rather

Corresponding author: martorjo@fis.upv.es

high temperatures (usually higher than 1000°C) during several days **[11]**. This method has several disadvantages such as inhomogeneities, lack of stoichiometric control and large particle size. These drawbacks can be avoided by synthesizing the materials using a solution-based method **[12]** where the mixing of different metal species occurs at a molecular level leading to the formation of polycrystalline homogeneous particles. In particular, $ZnCo_2O_4$ has been recently prepared by several solution-based methods including coprecipitation **[13]**, hydrothermal synthesis **[14]**, calcination of hydroxide or carbonate precursor mixtures **[15]**, electrophoretic deposition **[16]**, and sol-gel method **[17]**.

In this paper we report the deposition of thin films of spinel oxides by means of cathodic electrodeposition. This low-cost technique presents many advantages including the work at low temperatures (lower than 100°C) and at atmospheric pressure, the high homogeneity of the deposited films, the possibility of depositing large areas, and the direct monitoring of the deposited charge in order to control the film thickness. The main drawback is that a conducting substrate is required; however, this is not a problem for some applications of $ZnCo_2O_4$ like the use of this material as an oxygen (or chlorine) evolution electrode in solution **[18-20]**. We characterize the spinel thin films by means of Raman spectroscopy while most of the literature devoted to the spinel oxides dealt essentially with the infrared spectra of $A^{II}B^{III}{}_2O_4$ materials.

2. Experimental details

Ternary $Zn_xCo_yO_z$ and $Zn_xMn_yO_z$ films have been growth by electrodeposition onto ITO-coated glass substrate. The experimental setup used is basically composed by a computer-controlled potentiostat/galvanostat and a classical three-electrode electrochemical cell filled with a solution containing 0.1 M $KClO_4$ as supporting electrolyte and dissolved oxygen in a DMSO solution. Zn and Co chlorides are used as precursors: $ZnCl_2$, $CoCl_2$ and $MnCl_2$ in different concentrations. Pt and Ag/AgCl electrodes are used as counter electrode and reference electrode, respectively. The deposition potential was fixed at -0.9V and the solution temperatures are fixed at 900°C by a thermostat. This experimental setup has been previously used for the growth of wurzite-type ZnO-based ternary thin films with a high transparency and homogeneity **[21-24]**. The chemical composition has been determined by energy dispersive spectroscopy (EDS) and the structural characterization has been performed by x-ray diffraction (XRD) measurements. Finally, joint chemical and structural information has been obtained from Raman scattering measurements. For EDS measurements, we have used a JEOL-JSM 6300 scanning electron microscope. For XRD measurements we have used a high resolution

diffractometer system “Rigaku Ultima IV” using the copper anticathode (Cu Kα, λ = 1.542±0.002Å). Finally, for Raman measurements we have used a LabRAM HR UV system with a Peltier-cooled CCD camera and with have excited with the 532 nm laser line. The resolution of Raman scattering measurements is better than 2 cm^{-1}.

3. Results and discussion

Figure 1 shows the EDS results where the molar fraction x (x=[M]/([M]+[Zn])) of the M (M=Co, Mn) ions in the ZnO films is represented as a function of the molar fraction of M in the initial solution. EDS results confirm that the M ions incorporate into the ZnO lattice. The different experimental points of **Fig. 1** can be fitted with a Boltzmann function. Three different zones have been observed as a function of the initial molar fraction of the M ions in the solution: the first zone (for values lower than 0.1 for Co and 0.3 for Mn), where the curve has small slope; the second region (for values between 0.1 and 0.6 for Co and 0.3 and 0.6 for Mn), where the curve has a big slope; and finally, the third part for values larger than 0.6, where the curve has a small slope. The first zone is characterized by a small rate of incorporation of the M ions into the wurtzite ZnO lattice and this leads to the formation of M-doped ZnO with molar fractions in the films below 10%. The second region, where the curve has a steep slope, is characterized by a strong incorporation of the M ions in the ZnO lattice well above the solubility limit of the M ions in the wurtzite lattice and it is the zone where the formation of ZnM_2O_4 spinels takes place. Finally, the third part is a flat zone where the molar fraction of the M ions in the films remains constant despite increasing the concentration in the initial solution. In this region occurs the formation of pure M_3O_4 spinels, as we will show in the following paragraphs.

Figures 2(a) and (b) show the XRD patterns for samples of $Zn_{1-x}M_xO$ with different Co and Mn molar fractions in the films, respectively. The peaks with the symbol (*) belong to the ITO substrate. In both figures the peaks placed in 34.42º and 36.25º correspond to crystallographic directions (002) and (101) of the ZnO wurtzite structure. Our $Zn_{1-x}M_xO$ thin films grow preferentially along the (002) direction but this preferential direction of growth is reduced with increasing M concentration and at molar fractions above 10% the (101) direction is preferred. The wurtzite diffraction peaks disappear of the XRD patterns for molar fractions larger than 20% for Co and larger 30% for Mn in the films. It is rather curious beyond these molar fractions no XRD peaks are observed from the films even at the highest M

concentrations. Therefore, this result suggests that our films are amorphous or strongly disordered. Consequently, we have resorted to Raman spectroscopy to determine the possibly structure of the thin films with high M concentrations.

According to group theory, cubic spinels have the following phonon modes at the Γ point **[25]**

$$\Gamma = A_{1g}(R) + E_g(R) + 3T_{2g}(R) + 5T_{1u}(IR) + T_{1g} + 2A_{2u} + 2E_u + 2T_{2u}$$

where R and IR corresponds to Raman- and infrared-active modes, respectively, where one triply degenerated T_{1u} correspond to acoustic modes, and T_{1g}, E_u, A_{2u}, and T_{2u} are silent modes. Therefore, five Raman-active modes are expected in this structure. **Figure 3 (a) and (b)** show the results of different Raman spectra for samples with high Co and Mn concentrations, respectively. **Figure 3(a)** exhibits two different types of Raman spectra that can be related to two different compounds, namely the $ZnCo_2O_4$ and the Co_3O_4 spinels. For Co molar fractions in the films higher than 90% five narrow Raman modes are appreciated whose frequencies match with the Raman-active modes of the pure Co_3O_4 spinel as reported in the literature **[26]** (see values in **Table 1**). The small frequency changes between our samples and those reported in the literature are probably due to the Zn impurities present in our samples.

For molar fractions of Co below 90% the Raman spectra is formally identical to the $ZnCo_2O_4$ films of spinel structure already reported in the literature **[27]** (see **Table 1**). It can be observed that more than five Raman-active modes appear in the spectra. We think that the additional Raman modes (peaks marked with the asterisk in **Fig. 3(a)** and **Table 1)** occur because of the inversion of spinels. The mixture of cations in both crystal positions can produce the splitting of Raman modes to higher or lower frequency depending on the contribution of the cations to each Raman mode and the mass of each cation. In particular, the Raman T_{2g} mode at lowest frequency around 193 cm^{-1} in Co_3O_4 splits into two modes at 185 and 204 cm^{-1} in $ZnCo_2O_4$. The mode at 193 cm^{-1} in Co_3O_4 is a stretching mode in AB_2O_4 spinels related to A-O vibrations, and therefore is mainly contributed by Co ions in tetrahedral position in Co_3O_4 **[28]**. In this sense, one can understand that the mode at 185 cm^{-1} in $ZnCo_2O_4$ could be due to the occupation of tetrahedral sites by Zn, which has a slightly larger mass than Co, and that the small broad band around 204 cm^{-1} mode could be a signature of residual Co atoms in the tetrahedral sites in partially-inversed $ZnCo_2O_4$. Contrarily, the Raman A_{1g} mode at highest frequency around 682 cm^{-1} in Co_3O_4 splits into two modes at 661 and 686 cm^{-1} in $ZnCo_2O_4$. Since the A_{1g} mode is a B-O stretching mode in AB_2O_4 spinels which is mainly

contributed by the Co in octahedral coordination in Co_3O_4 **[28]**, the mode at 686 cm^{-1} in $ZnCo_2O_4$ seems to indicate the presence of Co in octahedral coordination while the broad band at 661 cm^{-1} would evidence the presence of a considerable amount of Zn ions in octahedral coordination.

As already commented, manganese oxide spinels (AMn_2O_4) typically have tetragonal spinel structure **[29]**. According to group theory, tetragonal spinels have the following phonon modes at the Γ point **[30]**

$$\Gamma = 2A_{1g}(R) + 3B_{1g}(R) + B_{2g}(R) + 4E_g(R) + 5A_{2u}(IR) + 7E_u(IR) + 2A_{1u} + A_{2g} + 2B_{2u}$$

where R and IR corresponds to Raman- and infrared-active modes, respectively, where one A_{2u} and one double degenerate E_u correspond to acoustic modes, and where A_{1u}, A_{2g}, and B_{2u} are silent modes. Therefore, ten Raman-active modes are expected in this structure. **Figure 3(b)** displays the Raman spectra for different samples with high Mn concentrations. It is observed that the Raman spectra can be classified again into two different classes. The first type of Raman spectra occurs for molar fractions of Mn between 66% and 78% and they correspond to a mixed spinel structure of $ZnMn_2O_4$ with tetragonal symmetry since similar bands to ours have been reported by Malavasi *et al.* **[28]** which have been summarized in **Table 2**. Black upward arrows in **Fig. 3(b)** mark the frequencies of the Raman modes of $ZnMn_2O_4$ reported by *Malavasi et al.* for comparison with our spectra. In order to show how we have obtained the frequencies reported in **Table 2** for $ZnMn_2O_4$ we show in **Figure 4 (a)** a decomposition of the Raman spectrum of $ZnMn_2O_4$, assuming that this stoichiometry is close to our sample with molar fraction x=0.66. It can be observed that we have fitted up to 8 peaks out of the 10 allowed Raman modes, whose frequencies compare reasonably with those of the five peaks reported in **Ref. 28**. Note that the frequencies of our $ZnMn_2O_4$ samples can be considerably affected by lack of stoichiometry. In fact, it can be observed that there is a shift of the Raman modes for higher Mn molar fractions than x=0.66 and that our frequencies are shifted with respect to those reported by Malavasi *et al.* **[28]**. These results suggest that our samples with x>0.66 have an excess of Mn with respect to the $ZnMn_2O_4$ stoichiometry.

The second class of Raman spectra correspond to the three samples with Mn molar fraction above x=0.85 in the films where the Raman spectrum is dominated by two broad bands. We have ascribed this sample to the spinel Mn_3O_4 whose frequencies are summarized in **Table 2** and compared to those present in the literature. In order to show how we have

obtained the frequencies reported in **Table 2** for Mn_3O_4 we show in **Figure 4 (b)** a decomposition of the Raman spectrum of Mn_3O_4 assuming that this stoichiometry is close to our sample with x=0.95. We have fitted up to 7 peaks out of the 10 allowed Raman modes, whose frequencies compare reasonably with those of the five peaks reported in **Ref. 28** for Mn_3O_4. In **Fig. 3(b)**, we have marked with red downward arrows the frequencies of the stronger bands of the Mn_3O_4 spinel reported by Lutz *et al.* and Malavasi *et al.* **[28,31]**. The frequencies of the Raman bands observed in our films with the highest Mn concentration match reasonably well with the frequencies of the Raman bands of the observed by other authors (see **Table 2**). Note that in our Mn_3O_4 films the fourth and five peaks reported by Malavasi *et al.* are observed as a broad band ranging from 250 to 350 cm^{-1} where three Gaussians can be fitted around 278, 301, and 334 cm^{-1}. Similarly, the broad band ranging from 520 to 700 cm^{-1} in our films has been fitted to two Gaussian profiles, being the stronger in intensity at a frequency of 645 cm^{-1}, which is close to the value reported for the strongest Raman peak of Mn_3O_4 (660 cm^{-1}).

Finally, we want to stress that the strongly broadened Raman bands of the films with the two highest Mn concentrations suggest the formation of strongly deformed or amorphous structures of tetragonal Mn_3O_4 spinel as compared to the narrow peaks reported in **Ref. 28**. However, we are confident that our films with the highest Mn concentrations correspond to the Mn_3O_4 spinel because the magnetisation curves that have been measured in our previous work exhibit the same magnetisation properties than Mn_3O_4 spinel **[32]**.

4. Conclusions

Spinel-type ZnM_2O_4 and M_3O_4 (M=Mn,Co) thin films have been obtained by electrodeposition with high transparency and homogeneity. EDS results confirm the incorporation of the Co or Mn ions in the ZnO lattice. Up to 20% at. Co and 10% at. Mn can be incorporated into the wurtzite ZnO lattice, whereas above those limits spinel-type compounds are formed as evidenced by Raman scattering measurements. At intermediate M molar fractions in the initial solution spinel-type ZnM_2O_4 is formed, while at high M concentrations pure M_3O_4 spinel is formed. The narrow Raman peaks of Co_3O_4 indicate that this pure spinel has rather good crystal quality while the broad Raman peaks of Mn_3O_4 suggest that this pure spinel has a bad crystal quality.

Acknowledgements

The authors are grateful to Ministerio de Ciencia e Innovación of Spain (MICINN) under the National Program of Materials (MAT2007-65990-C03-02 and MAT2010-21270-C04-04) and the Consolider-Ingenio 2010 Program (MALTA CSD2007-0045).

References

[1] J. Ghose, K.S.R.C. Murthy, J. Catal. **162**, 359 (1996).
[2] N. Guilhaume, M. Primet, J. Chem. Soc. Faraday Trans. **90**, 1541 (1994).
[3] B.L. Yang, D.S. Chen, S.B. Lee, Appl. Catal. **70**, 161 (1991).
[4] J.P. Jacobs, A. Maltha, J.G. H. Reinthjes, J. Drimal, V. Ponec, H.H. Brongersma, J. Catal. **147**, 294 (1994).
[5] J. Sloczynski, J. Ziólkovski, B. Grzybowska, R. Grabowski, D. Jachewicz, K. Wcislo, and L. Gengembre, J. Catal. **187**, 410 (1999).
[6] C. Ai, M. Yin, C. Wang, and J. Sun, J. Mat. Sci. **39**, 1077 (2004).
[7] Y. Sharma, N. Sharma, G.V. Subba Rao, and B.V.R. Chowdari, Adv. Funct. Mat. **17**, 2855 (2007).
[8] X. Niu, W.P. Du, and W.M. Du, Sensors & Actuators B **99**, 405 (2004).
[9] W.M. Shaheen and A.A. Ali, Materials Research Bulletin **36**, 1703 (2001).
[10] D. Jarosch, Mineralogy and Petrology **37**, 15 (1987).
[11] C. Otero Areán, M. Peñarroya Mentruit, A.J. López López, J.B. Barra, Phys. Eng. Aspects **180**, 253 (2001).
[12] A. Manthiram and J. Kim, Chem. Mater. **10**, 2895 (1998).
[13] K.L. Zhang, J.B. Yuan, G.F. Zhu, Q.C. Zhang, J.T. Tang, J. Wuhan Univ. (Nat. Sci. Ed.) **4**, 428 (1997).
[14] A.G. Shi, A.H. Hang, J. Fang, J.S. Chi, M.M. Wu, Chin. J. Inorg. Chem. Ind. **5**, 14 (2001).
[15] K.J. Omata, T.K.S. Takada, S.J. Kasahara, M.N.Y.S. Yamada, Appl. Catal. A:Gen. **146**, 255 (1996).
[16] B. Chi, J. Li, X. Yang, H. Lin, and N. Wang, Electrochim. Acta **50**, 2059 (2005).
[17] X. Wei, D. Chen, and W. Tang, Mat. Chem. Phys. **103**, 54 (2007).
[18] S. Trasatti, G. Lodi in: S. Trasatti (Ed.), Electrodes of Conductive Metallic Oxides, Part A, Elsevier, Amsterdam, 1980.
[19] P. Rasiyah, A.C.C. Tseung, D.B. Hibbert, J. Electrochem. Soc.: Electrochem. Sci. Techhol. **129**, 1724 (1982).
[20] R.N. Singh, J.-F. Koenig, G. Poillerat, P. Chartier, J. Electrochem. Soc. **137**, 1408 (1990).
[21] M. Tortosa, M. Mollar, and B. Marí, J. Cryst. Growth **304**, 97 (2007).
[22] M. Tortosa, M. Mollar, and B. Marí, Physica Status Solidi (C) **5**, 3467 (2008).
[23] B. Marí, J. Cembrero, M. Mollar, and M. Tortosa, Physica Status Solidi (C) **5**, 555 (2008).
[24] M. Tortosa, M. Mollar, B. Marí, and F. Lloret, J. Appl. Phys. **104**, 033901 (2008).
[25] A. Chopelas and A. Hofmeister, Phys. Chem. Miner. **18**, 279 (1991).
[26] V.G. Hadjiev, M.N. Iliev, and I.V. Vergilov, J. Phys. C: Solid State Phys. **21**, 199 (1988).

[27] K. Samanta, P. Bhattacharya, R.S. Katiyar, W. Iwamoto, P.G. Pagliuso, and C. Rettori, Phys. Rev. B **73**, 245213 (2006).
[28] L. Malavasi, P. Galinetto, M.C. Mozzati, C.B. Azzoni, and G. Flor, Phys. Chem. Chem. Phys. **4**, 3876 (2002).
[29] M. Nogues and P. Poix, Ann. Chim. (Paris) **1972**, 301 (1972).
[30] Bilbao Crystallographic Server, http://www.cryst.ehu.es
[31] H.D. Lutz, B. Müller, and H.J. Steiner, J. Solid State Chem. **90**, 54 (1991).
[32] M. Mollar, M. Tortosa, R. Casasús, B. Marí, Microelectronics Journal **40**, 276-279 (2009).

Table 1 Frequencies and symmetries of Raman modes observed in $ZnCo_2O_4$ (x=0.58) thin films compared to those reported in the literature (**Ref. 27**) and of Co_3O_4 (x=0.99) thin films compared to those reported in the literature (**Ref. 5**).

Phonon symmetry	Frequency (cm^{-1}) $ZnCo_2O_4$ (x=0.58)	Frequency (cm^{-1}) $ZnCo_2O_4$ (Ref. 27)	Frequency (cm^{-1}) Co_3O_4 (x=0.99)	Frequency (cm^{-1}) Co_3O_4 (Ref. 5)
T_{2g}	193	193	193	194.4
E_g	476	476	476	482.4
T_{2g}	517	517	517	521.6
T_{2g}	615	615	615	618.4
A_{1g}	683	683	683	691.0
*	204	200		
*	661	660		

Table 2 Frequencies and symmetries of Raman modes observed in $ZnMn_2O_4$ (x=0.66) and of Mn_3O_4 (x=0.95) thin films compared to those reported in the literature (**Ref. 28**).

Phonon mode	Frequency (cm^{-1}) $ZnMn_2O_4$ (x=0.66)	Frequency (cm^{-1}) $ZnMn_2O_4$ (Ref. 28)	Frequency (cm^{-1}) Mn_3O_4 (x=0.95)	Frequency (cm^{-1}) Mn_3O_4 (Ref. 28)
Peak 1	276	300.2	278	
Peak 2	316	320.5	301	290
Peak 3	320		334	319
Peak 4	369	381.9	405	374
Peak 5	463	475.5	474	479
Peak 6	563		599	
Peak 7	630			
Peak 8	663	677.6	645	660

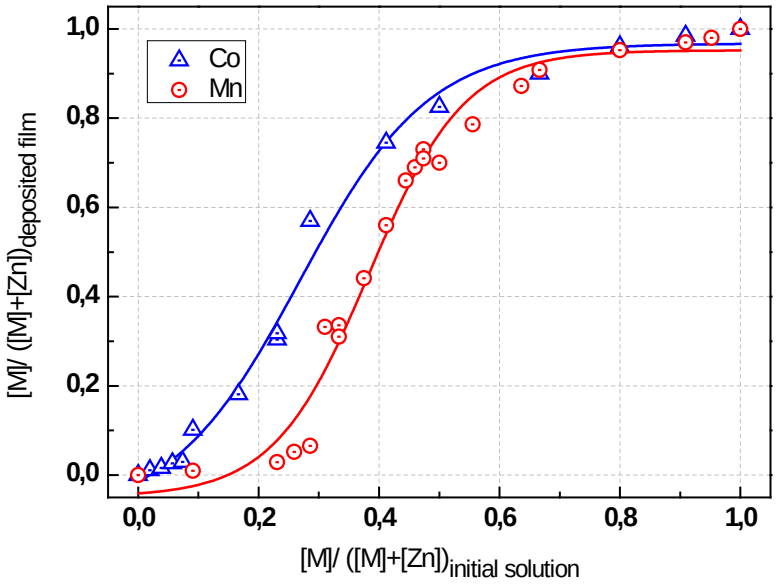

Figure 1 Molar fraction x=[M]/([M]+[Zn]) in the deposited film as a function of the molar fraction in the initial solution.

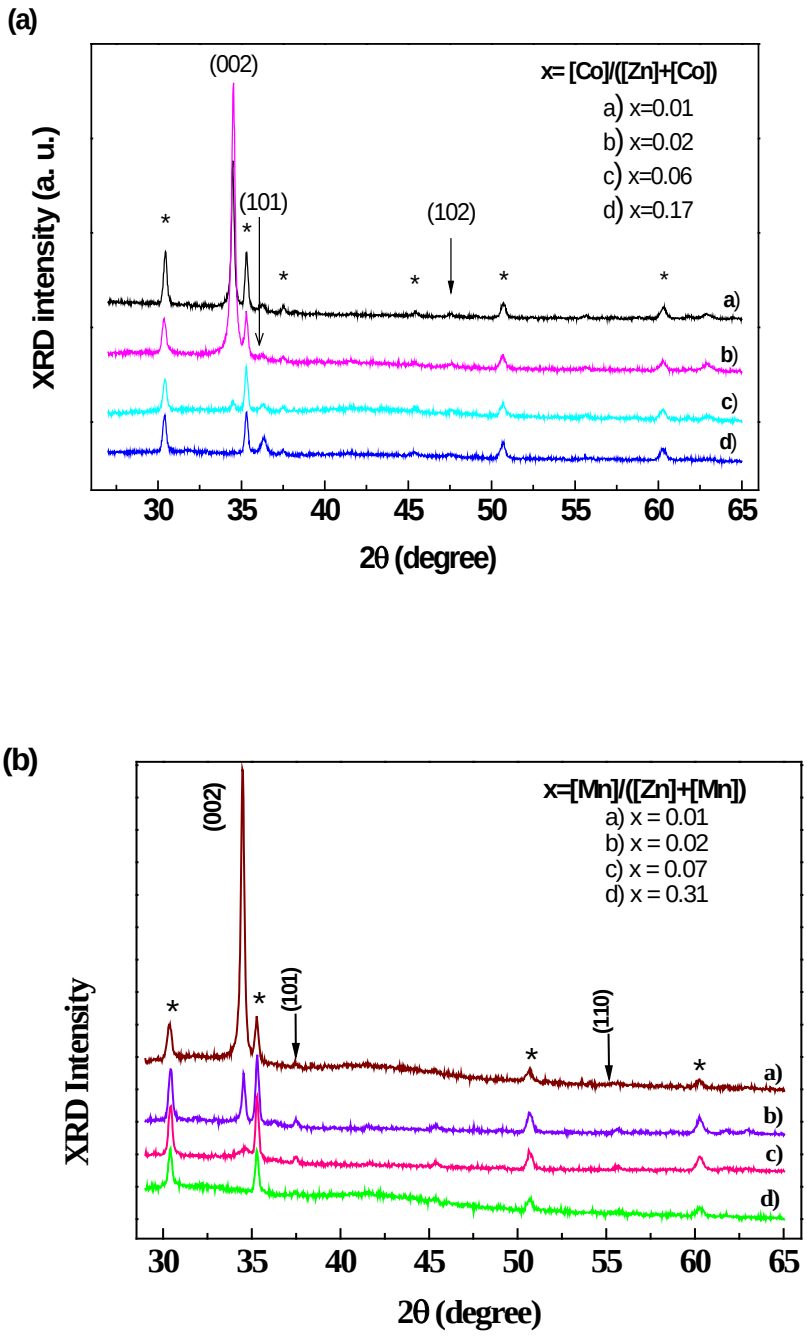

Figure 2 (a) XRD scan diagram of $Zn_{1-x}Co_xO$ films for different Co molar fractions, (b) XRD scan diagram of $Zn_{1-x}Mn_xO$ films for different Mn molar fractions. Asterisks correspond to XRD peaks of ITO substrate.

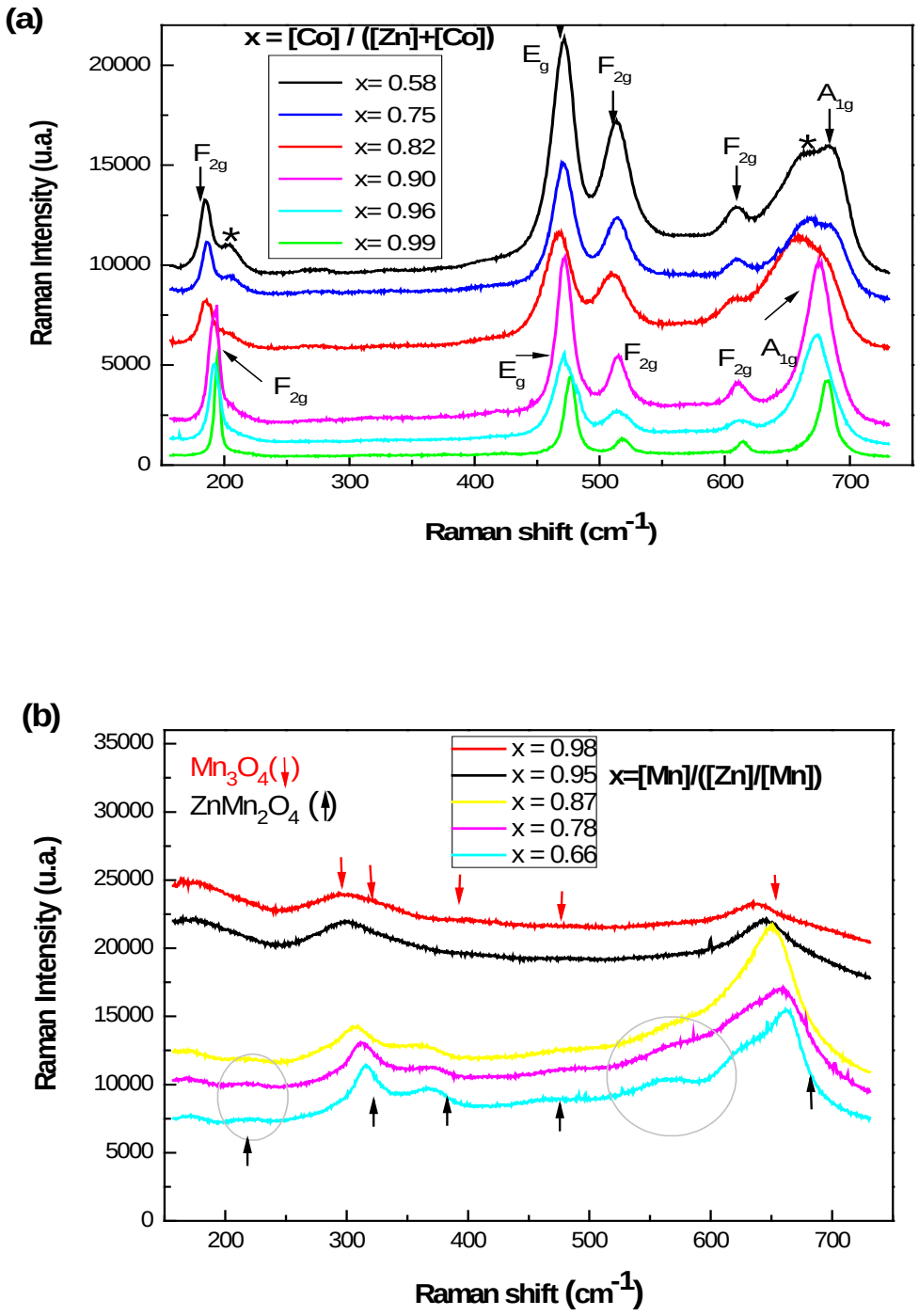

Figure 3. (a) Raman spectra of thin films with different molar fractions of Co in the films. (**b)** Raman spectra of thin films for different molar fractions of Mn in the films.

(a)

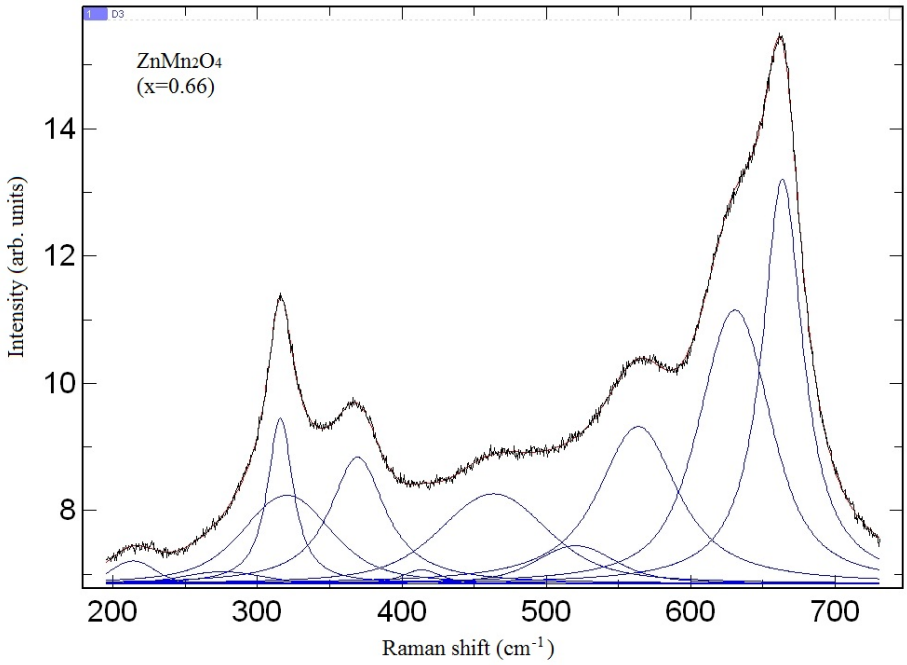

(b)

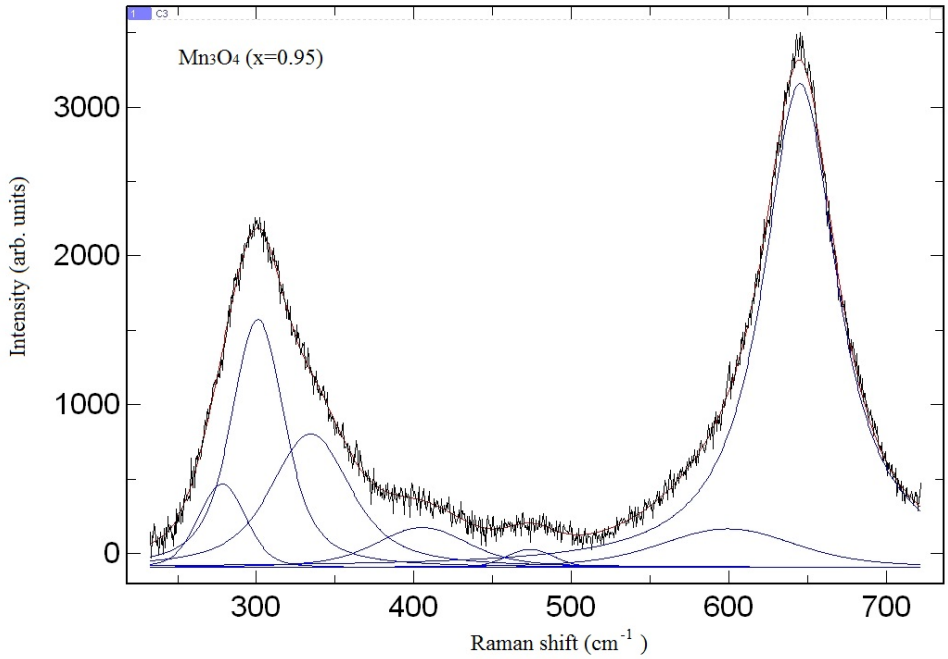

Figure 4. (a) Raman spectra of a thin film with a Mn molar fraction of 0.66 ($ZnMn_2O_4$) decomposed into Gaussian profiles. **(b)** Raman spectra of a thin film with a Mn molar fraction of 0.95 (Mn_3O_4) decomposed into Gaussian profiles.